



ARTICLE

Bavachin protects against diet-induced hepatic steatosis and obesity in mice

Xiang Wei^{1,2}, Li Lin¹, Qian-qian Yuan¹, Xiu-yun Wang¹, Qing Zhang¹, Xiao-min Zhang¹, Ke-chao Tang¹, Man-yu Guo¹, Ting-yu Dong³, Wei Han⁴, Da-ke Huang⁵, Yin-liang Qi², Mei Zhang⁶✉ and Hua-bing Zhang^{1,7}✉

Non-alcoholic fatty liver disease (NAFLD) is a major health concern worldwide, and the incidence of metabolic disorders associated with NAFLD is rapidly increasing because of the obesity epidemic. There are currently no approved drugs that prevent or treat NAFLD. Recent evidence shows that bavachin, a flavonoid isolated from the seeds and fruits of *Psoralea corylifolia* L., increases the transcriptional activity of PPAR γ and insulin sensitivity during preadipocyte differentiation, but the effect of bavachin on glucose and lipid metabolism remains unclear. In the current study we investigated the effects of bavachin on obesity-associated NAFLD in vivo and in vitro. In mouse primary hepatocytes and Huh7 cells, treatment with bavachin (20 μ M) significantly suppressed PA/OA or high glucose/high insulin-induced increases in the expression of fatty acid synthesis-related genes and the number and size of lipid droplets. Furthermore, bavachin treatment markedly elevated the phosphorylation levels of AKT and GSK-3 β , improving the insulin signaling activity in the cells. In HFD-induced obese mice, administration of bavachin (30 mg/kg, *i.p.* every other day for 8 weeks) efficiently attenuated the increases in body weight, liver weight, blood glucose, and liver and serum triglyceride contents. Moreover, bavachin administration significantly alleviated hepatic inflammation and ameliorated HFD-induced glucose intolerance and insulin resistance. We demonstrated that bavachin protected against HFD-induced obesity by inducing fat thermogenesis and browning subcutaneous white adipose tissue (subWAT). We revealed that bavachin repressed the expression of lipid synthesis genes in the liver of obese mice, while promoting the expression of thermogenesis, browning, and mitochondrial respiration-related genes in subWAT and brown adipose tissue (BAT) in the mice. In conclusion, bavachin attenuates hepatic steatosis and obesity by repressing de novo lipogenesis, inducing fat thermogenesis and browning subWAT, suggesting that bavachin is a potential drug for NAFLD therapy.

Keywords: non-alcoholic fatty liver disease; obesity; bavachin; lipogenesis; insulin sensitivity; AKT; GSK-3 β ; thermogenesis; subcutaneous white adipose tissue; mouse primary hepatocytes

Acta Pharmacologica Sinica (2023) 44:1416–1428; <https://doi.org/10.1038/s41401-023-01056-z>

INTRODUCTION

Non-alcoholic fatty liver disease (NAFLD) is the leading cause of chronic liver disease worldwide, and is characterized by hepatic fat accumulation in the absence of excessive alcohol consumption or other attributable causes, with the presence of steatosis in at least 5% of hepatocytes [1, 2]. In the last few decades, the prevalence of NAFLD has accounted for approximately 25% of the world's population, rising to become a global public health concern [3]. The rising incidence of NAFLD is strongly associated with the increase in the prevalence of obesity, dyslipidemia, and type II diabetes mellitus (T2DM). In the absence of intervention, NAFLD will eventually worsen and develop into non-alcoholic steatohepatitis (NASH), cirrhosis, and even hepatocellular carcinoma (HCC) [4]. To date, no approved effective drugs are available to prevent

or treat NAFLD, although over 25 medications are currently in the phase 2 or 3 of clinical trial [4]. Lifestyle modifications, diet, and physical activity are currently recommended as effective interventions for the treatment of NAFLD, while therapeutic disease-modifying options for patients with NAFLD are limited. Therefore, an unmet medical need exists to develop new drugs to treat NAFLD.

The search for natural compounds with high efficiency and low toxicity has become a trend in drug development and clinical medicine. Compared with Western medicines, traditional Chinese medicines have attracted significant attention in recent years for the treatment of NAFLD because of their multi-target and multi-channel action mechanisms [5]. Recently, a variety of traditional Chinese medicine monomers have been found to exhibit

¹Department of Biochemistry and Molecular Biology, Metabolic Disease Research Center, School of Basic Medicine, Anhui Medical University, Hefei 230032, China; ²Department of Hyperbaric Oxygen, The Second People's Hospital of Hefei, Hefei Hospital Affiliated to Anhui Medical University, Hefei 230011, China; ³The Second Clinical Medical College of Anhui Medical University, Hefei 230032, China; ⁴Department of Gastroenterology, The First Affiliated Hospital of Anhui Medical University, Hefei 230022, China; ⁵Synthetic Laboratory of School of Basic Medicine Sciences, Anhui Medical University, Hefei 230032, China; ⁶Health Management Center, The First Affiliated Hospital of the University of Sciences and Technology of China (Anhui Provincial Hospital), Hefei 230001, China and ⁷The Affiliated Chuzhou Hospital of Anhui Medical University (The First People's Hospital of Chuzhou), Chuzhou 239001, China

Correspondence: Mei Zhang (syzm110011@163.com) or Hua-bing Zhang (huabingzhang@ahmu.edu.cn)

These authors contributed equally: Xiang Wei, Li Lin, Qian-qian Yuan

Received: 8 September 2022 Accepted: 13 January 2023

Published online: 31 January 2023

hepatoprotective effects, modulating lipid metabolism, insulin resistance, and anti-inflammatory and anti-oxidant effects. These drugs can be broadly classified into five categories: [6] 1) phenols, represented by resveratrol [7] and curcumin; [8] 2) terpenoids, represented by paeoniflorin; [9] 3) flavonoids, represented by baicalin [10] and puerarin; [11] 4) alkaloids, represented by berberine; [12, 13] and 5) others. Recently, gastrodin and salidroside have been demonstrated to protect against high-fat diet (HFD)-induced NAFLD and NASH progression by regulating the AMP-activated protein kinase (AMPK) signaling pathway [14, 15]. Bavachin is a bioactive natural flavonoid widely used in traditional medicine and is isolated from the seeds and fruits of *Psoralea corylifolia* L [16]. Bavachin has been reported to have anti-tumor, anti-oxidant, anti-inflammatory, immunomodulatory, and estrogenic activities [16]. Furthermore, a previous study reported that bavachin improved the insulin-dependent glucose uptake in differentiated adipocytes and myoblasts [17]. Moreover, it has been reported that bavachin increased the peroxisome proliferator-activated receptor γ (PPAR γ) transcriptional activity during preadipocyte differentiation and increased the insulin sensitivity by regulating the AMPK and protein kinase B (AKT) signaling pathways. However, the effects of bavachin on glucose and lipid metabolisms remain unclear.

In this study, we revealed that bavachin not only reduced the hepatic lipid accumulation, inflammatory response, and endoplasmic reticulum (ER) stress, but also increased the insulin sensitivity in the liver, fat, and muscle of HFD-fed mice. Moreover, our results identified that bavachin may protect against HFD-induced obesity by inducing fat thermogenesis and beige subcutaneous white adipose tissue (subWAT). In addition, we found that bavachin attenuated palmitic acid (PA)/oleic acid (OA) stimulated lipid accumulation in mouse primary hepatocytes and Huh7 cells in vitro and alleviated insulin resistance. Our data suggest that bavachin could be a novel therapeutic agent to combat metabolic diseases.

MATERIALS AND METHODS

Animal model

C57BL/6 J mice (4-week-old male) were obtained from Gempharmatech Co., Ltd, China. All mice were maintained under standard conditions of humidity and temperature with a 12:12 h light:dark cycle. After adaptation for one week, the mice were randomly divided into four groups and fed for 20 weeks as follows: normal diet ($n = 3$), HFD-induced obese mice with dimethyl sulfoxide (DMSO) ($n = 6$), HFD with bavachin (30 mg/kg body weight every second day, $n = 8$), and HFD with rosuvastatin calcium (Medchemexpress, HY-17504/CS-2111, China) (10 mg/kg body weight every second day, $n = 5$). The HFD was fed to all males in the control, bavachin and rosuvastatin calcium groups for 20 weeks. From the thirteenth week, the control group received intraperitoneal injections of normal saline, while the Bavachin group received intraperitoneal injections of bavachin, and the rosuvastatin calcium group received intraperitoneal injections of rosuvastatin calcium. Unless otherwise noted, male mice were used for all experiments. All animal experiments conformed to the guidelines of the Animal Center of Anhui Medical University. The experimental protocols used on animals were approved by the Institutional Animal Care and Use Committee of Anhui Medical University.

Reagents and materials

Fetal bovine serum (FBS) was purchased from Lonsera (S711-001S, Uruguay), while Roswell Park Memorial Institute (RPMI)-1640 (C11875500BT, China) and Dulbecco's modified Eagle's medium (DMEM, high glucose) (C11965500BT, China) were obtained from Gibco and DMEM:F-12 (DMEM/F-12) (01-172-1ACS, China) was obtained from Biological industries. Bavachin was purchased from

Medchemexpress (HY-N0233/CS-6113, China). PA (408-35-5), OA (143-19-1) and insulin (Ins, 11070-73-8) were purchased from Sigma Aldrich, Missouri, USA. The high-fat diet with 60% kcal chow that was fed to the rodent mice was obtained from Changzhou SYSE Bio-tec Co. Ltd (PD6001, China).

Cell culture and treatment

Mouse primary hepatocytes were isolated from the livers of 6–8 week-old male C57BL/6 J mice. Huh7 cells, human hepatocyte-derived liver cells (L02) and immortalized normal hepatocyte AML12 of mice were stored in the laboratory for long-term storage. Primary hepatocytes and L02 cells were cultured in RPMI-1640 with 10% FBS, 100 U/mL penicillin and 0.1 mg/mL streptomycin (Beyotime, C0222, China) at 37 °C in a humidified incubator containing 5% CO₂. Huh7 cells were cultured in DMEM and AML12 cells were cultured in DMEM/F12 under identical conditions. The cells were treated with 0.2 mM PA and 0.1 mM OA or 30 mM glucose (Sangon Biotech, 50-99-7, China) and 100 nM insulin for 24 h to create a hepatocyte steatosis model in vitro, in which, PA/OA or high glucose and high insulin (HG/HIn) was treated for 12 h and then bavachin was added to continue the treatment for 12 h.

Cell viability assay

Viability assays of primary hepatocytes and Huh7 cells were performed using the methyl thiazolyl blue tetrazolium bromide (MTT) (Solarbio Life, 298-93-1, China) method. Cells were first exposed to different concentrations of bavachin (10, 20, 30, and 40 μ M). After the indicated treatment, MTT was added at a working concentration of 5 mg/mL, and the solution was incubated for 4 h. Next, the MTT solution was removed and 100 μ L/well of DMSO was added to dissolve the needle-like formazan crystals formed by viable cells. The absorbance was measured at 490 nm, and the percentage of cell viability was calculated.

Cell and tissue Oil Red O staining

Cellular lipid content was visualized by Oil Red O staining. The cells were washed twice with phosphate buffer solution (PBS), fixed in 4% paraformaldehyde for 1 h and re-washed twice with PBS. The samples were then soaked in 60% isopropanol for 3–5 min, and stained with freshly prepared Oil Red O staining solution for 10 min. After washing twice with PBS, the red-stained lipid droplets were observed and imaged using a light microscope (Olympus, DP80, Japan) at $\times 400$ magnification. After staining with an Oil Red working solution and rewashing with PBS, the frozen tissue sections were counterstained with hematoxylin for 80 s. The sections were then rinsed with running water for 10 min, and lipid droplets were observed under a microscope.

Tissue and cellular triglyceride assays

To quantify the tissue and intracellular lipid accumulation, the TG content in primary hepatocytes, Huh7 cells, and the liver was measured using a TG content assay kit (Applygen Technologies, Inc., Beijing, China, E1013). The tissue and cells were lysed to obtain the supernatant according to the manufacturer's instructions. After mixing 10 μ L of supernatant with 190 μ L of chromogenic solution, the absorbance at 550 nm was measured using a microplate reader (Thermo fisher scientific, 1510, Massachusetts, USA). The corresponding TG content was calculated according to the instruction manual.

Hematoxylin-eosin staining

After the paraffin sections were gradient dewaxed in xylene and ethanol, the nuclei were stained with hematoxylin for 5 min, washed with water, immersed in eosin solution for 15 s, re-washed with water, and dried at 55 °C. After fixing with neutral resin sealing tablets and drying, the stained sections were observed and photographed under a microscope.

Table 1. RT-PCR primers.

Mouse (gene)	Forward Primer (5'-3')	Reverse Primer (5'-3')
SREBP-1c	GGAGCCATGGATTGCACATT	GGCCAGGGAAGTCACTGT
FAS	GTAAGTTCTGTGGCTCCAGAG	GCCCTCCCGTACACTCACTC
ACC	AGGAAGATGGCGTCCGCTCTG	GGTGAGATGTGCTGGGTCAT
SCD-1	CTGCACCTCCCTCCGAAAT	TCCTCCAGACGTACTCCAGC
PPAR γ	GCATGGTGCCTTCGCTGATGC	AGGCCTGTTGTAGAGCTGGGT
PPAR α	ACAAGGCCTCAGGGTACCA	GCCGAAAGAAGCCCTTACAG
CPT-1 α	GAACCCCAACATCCCAAAAC	TCCTGGCATTCTCCTGGAAT
CD36	TCCCTTGGCAACCAACCAC	TCCACCAGTTGCTCCACAC
MTTP	AGTGCAGTTCTCACAGTACCCGTT	AGCATATCGTTCTGGTGAAGGGA
PLIN2	CAATTTGTGGCTCCAGCTTC	CCCGTATTTGAGATCCGTGT
PEPCK	GGTTCACAGGGTGCATGAAA	CACGTAGGGTGAATCCGTCAG
G6PC	AAGTCCTCTCCGACATCCAG	GTCTCACAGGTGACAGGGAAC
TNF α	CGTCAGCCGATTGCTATCT	CGGACTCCGCAAAGTCTAAG
IL-6	AGTTGCCTTCTGGGACTGA	TCCACGATTTCCAGAGAAC
MCP1	TCTGGACCCATTCTTCTTG	AGGTCCTGTCATGCTTCTG
IL-1 β	TGAAGTTGACGGACCCCAAAA	TGATGTGCTGCTCGGAGATT
UCP1	ATTCAGAGGCAAATCAGCTTTG	GTGTTTCTCTCCCTGAAGAGAA
Prdm16	CAACAAAGAGAAGCCGTTCAAG	TTTCGGATCTCGGAGAAGTAAG
PGC-1 α	TGGACGGAAGCAATTTTTCA	TTACTGCGCAAGCTTCTCT
Cidea	CAATGTCAAAGCCACGATGTAC	CTGTGACGATAGGACATAAAC
Dio2	TTCTCCTCGGTGGTCTGACTTCC	GCACATCGGTCTCTTGGTTCC
Elov13	GGACCTGATGCAACCCTATG	CCAACAACGATGAGCAACAG
36B4	ATCCCTGACGCACCGCCGTGA	TGCATCTGCTTGGAGCCACGTT

Immunohistochemistry staining

Immunohistochemistry was performed to determine the levels of the macrophage marker F4/80 in mature mice. Paraffin sections were gradient dewaxed and sodium citrate was used for antigen repair. The sections were pretreated with an endogenous peroxidase blocker for 30 min to quench the endogenous peroxidase activity, and subsequently blocked in goat serum for 30 min. F4/80 staining was performed by incubating with the corresponding primary antibody (Proteintech, 28463-1-AP, China) in a humidified chamber at 4°C overnight. The sections were washed with PBS and incubated with goat anti-rat immunoglobulin G-horseradish peroxidase (IgG-HRP) for 30 min at 37°C. After diaminobenzidine (DAB) staining (ZSGB-BIO, ZLI-9017, China), observation and photography were performed under a microscope.

Glucose and insulin tolerance tests

The glucose tolerance test (GTT) was performed in mice that were fed a HFD, as described above. One day later, the mice were subjected to insulin tolerance tests (ITT). For the GTT, the mice underwent fasting for 16 h and were injected with a glucose solution in saline (1.0 g/kg body weight) intraperitoneally. For the ITT, the mice underwent fasting for 6 h and were injected with recombinant human insulin (1.0 U/kg body weight) intraperitoneally. Blood glucose levels were measured in the tail blood before or 15, 30, 45, 60, 90, and 120 min after glucose or insulin injections.

VLDL-TG secretion

Mice in each group were starved for 7–8 h and tyloxapol (500 mg/kg body weight, Macklin, 25301-02-4, China) was injected into the tail vein to inhibit very low density lipoprotein (VLDL) catabolism. Blood samples were drawn from the tail vein at 0, 1, 2, and 3 h after injection of tyloxapol. Plasma was isolated by centrifugation, after which the TG levels were determined as previously described.

Measurements of triglyceride, cholesterol, free fatty acids, ALT, AST, TNF α plasma levels

Following anesthetization, blood was collected from the orbit and the serum was separated at 3000 rpm for 10 min. Serum alanine aminotransferase (ALT), aspartate aminotransferase (AST), TG, total cholesterol (TC), and free fatty acid (FFA) levels were determined using an automated device (Monach) in the clinical laboratory of the First Affiliated Hospital of Anhui Medical University, Hefei, China. Serum tumor necrosis factor alpha (TNF- α) concentrations were determined by ELISA (Elabscience Biotechnology Inc, E-MSEL-M0002, China) testing.

Quantitative real-time PCR analysis

Total RNA was extracted from tissues or cells using the TRIzol reagent (Thermo fisher scientific, 15596026, Massachusetts, USA) and reverse transcribed into cDNA using the First Strand cDNA Synthesis Kit (Tolobio, # 22112, China), according to the manufacturer's instructions. Quantitative PCR (qPCR) analysis was performed using the SYBR Green PCR master mix (Tolobio, #22204, China) on a Light Cycler 96 (Roche, Switzerland) system to examine the expression of related genes. The primer sequences used for this reaction are listed in Table 1.

Western blot analysis

Primary hepatocytes, Huh7 cells, the liver, and adipose tissues were extracted in RIPA lysis buffer containing protease and phosphatase inhibitors. After centrifugation at 12,000 \times g for 15 min at 4°C, the supernatants were assayed to determine the protein concentration using the BCA method. The protein was solubilized in SDS loading buffer and heated in a metal bath for 10 min. Equal amounts of protein were separated by 10% SDS-PAGE and transferred onto PVDF membranes (Millipore, Missouri, USA, 0.45 μ m pore size). After sealing with 5% skimmed milk powder, the membranes were washed and incubated with the corresponding primary antibodies overnight at 4°C. After

Table 2. Primary antibodies.

Anti-body	Dilution ratio	Brands	Item No.	Country
AKT	1:1000	CST	#9272 S	Boston, USA
p-AKT	1:1000	CST	#9271 S	Boston, USA
GSK-3 β	1:1000	CST	#9315 S	Boston, USA
p-GSK-3 β	1:1000	CST	#5558 S	Boston, USA
ACC	1:1000	CST	#3676	Boston, USA
p62	1:1000	CST	#23214	Boston, USA
eIF-2 α	1:1000	CST	#5324 T	Boston, USA
p-eIF-2 α	1:1000	CST	#3398 T	Boston, USA
IRE-1 α	1:1000	CST	#3294 T	Boston, USA
JNK	1:1000	CST	#9252	Boston, USA
p-JNK	1:1000	CST	#4668	Boston, USA
NF- κ B	1:1000	CST	#8242 T	Boston, USA
p-NF- κ B	1:1000	CST	#3033 T	Boston, USA
α -tubulin	1:1000	CST	#2125	Boston, USA
FAS	1:1000	Santa	sc-74540	China
SREBP-1c	1:1000	Santa	sc-13551	China
CD36	1:500–1:1000	Abclonal	A5792	China
SCD-1	1:500–1:1000	Abclonal	A16429	China
p-IRE-1 α	1:1000	Abclonal	#AP0878	China
G6Pase	1:1000	Abclonal	A21168	China
MTPP	1:1000	BD Biosciences	612022	New Jersey, USA
PLIN2	1:1000	Proteintech	15294-1-AP	China
LC3	1:1000	Proteintech	14600-1-AP	China
CHOP	1:1000	Proteintech	15204-1-AP	China
PEPCK	1:1000	Proteintech	16754-1-AP	China
PGC-1 α	1:1000	Proteintech	66369-1-Ig	China
CPT-1 α	1:1000	Abcam	ab128568	UK
UCP1	1:1000	Abcam	ab10983	UK
XBP1	1:1000	BOSTER	#PB9463	China

incubation with corresponding secondary antibodies (Biomike, China, 1:10,000) for 1 h at room temperature, the signals were developed using an ECL luminescent kit (ZENBIO, #17046, China) and detected using an enhanced chemiluminescence detection system (Clinx, 3300 Mini, China). Primary antibodies applied in the study are listed in Table 2. The protein bands were analyzed using Quantity one (4.6.2), and α -tubulin protein was used as an internal control.

RNA sequencing

Transcriptome sequencing and analysis were conducted by OE Biotech Co. Ltd. (Shanghai, China). We collected liver sections from three mice, from the bavachin and control groups, for the purpose of sequencing. Total RNA was extracted using the mirVana miRNA Isolation Kit (Ambion), following the manufacturer's protocol. RNA integrity was evaluated using the Agilent 2100 Bioanalyzer (Agilent Technologies, Santa Clara, CA, USA). Samples with an RNA integrity number (RIN) ≥ 7 were subjected to subsequent analysis. Libraries were constructed using the TruSeq Stranded mRNA LTSample Prep Kit (Illumina, San Diego, CA, USA), according to the manufacturer's instructions and sequenced on an Illumina sequencing platform (HiSeqTM 2500 or Illumina HiSeq X Ten) where 125 bp/150 bp paired-end reads were generated. The RNA-sequencing (RNA-seq) data were deposited in National Center for Biotechnology Information (NCBI) under the SRA accession numbers (SRA: PRJNA872948).

Statistical analysis

All data are presented as mean \pm SEM for the experiments. Statistical analyses were performed using the GraphPad Prism software, version 8.6. Student's *t*-test or analysis of variance (one-way ANOVA) was used to evaluate the statistical differences: **P* < 0.05, ***P* < 0.01, and ****P* < 0.001 were considered statistically significant.

RESULTS

Bavachin represses cellular TG synthesis in primary hepatocytes of mice and Huh7 cells

Bavachin improves the insulin-dependent glucose uptake in differentiated adipocytes and myoblasts [17], the structure of which is shown in Fig. 1a. However, the role of bavachin in glucose and lipid metabolism remains unclear. In this study, we explored the role of bavachin in the regulation of lipid metabolism in the liver. The cells were treated with 20 μ M bavachin, considering its mechanism of modulating the cytotoxicity of mouse primary hepatocytes and Huh7 cells (Fig. 1b, c). In addition, we confirmed that PA/OA or HG/Hln treatments upregulated the expression of fatty acid synthesis-related genes in the mouse primary hepatocytes and Huh7 cells, while 20 μ M bavachin treatment reduced the expression of fatty acid synthesis genes (Supplementary Fig. S1a–d). Quantitative analysis demonstrated that bavachin inhibited TG synthesis in the mouse primary hepatocytes following PA/OA stimulation for 24 h (Fig. 1d). Furthermore, our results showed that bavachin reduced the number and size of PA/OA-induced lipid droplets in primary mouse hepatocytes (Fig. 1e). Next, we explored whether bavachin could reduce the hepatic expression of genes related to fatty acid synthesis in vitro. Western blotting results revealed that the protein expression levels of genes related to fatty acid synthesis, such as fatty acid synthase (FAS), acetyl-CoA carboxylase (ACC), and stearyl-coenzyme A desaturase 1 (SCD-1), were decreased in the primary mouse hepatocytes, when exposed to high concentrations of PA/OA treated with bavachin, compared to that in the control group. In addition, we also observed that the protein level of fatty acid translocase CD36 (CD36) was significantly reduced in the bavachin group compared to that in the control group (Fig. 1f). The same results were observed in Huh7 cells (Fig. 1g–i), as well as AML12 and L02 cells (Supplementary Fig. S1e–h).

Bavachin improves insulin sensitivity of hepatocytes in vitro

A previous study confirmed that bavachin increased the insulin sensitivity in 3T3-L cells [17]. Therefore, we examined whether bavachin affects the insulin activity in hepatocytes. The phosphorylation level of AKT, a key indicator of insulin signaling pathway activity, is crucial for the insulin-activated glucose absorption in the liver. Our results demonstrated that bavachin administration dramatically increased the phosphorylation of AKT in primary mouse hepatocytes (Fig. 2a, b) and Huh7 cells (Fig. 2c, d). Bavachin treatment markedly elevated the phosphorylation level of glycogen synthase kinase-3 β (GSK-3 β) downstream of AKT in primary hepatocytes (Fig. 2a, b) of mice and Huh7 cells (Fig. 2c, d). We observed the same effect on AML12 and L02 cells (Supplementary Fig. S2a–d), suggesting that bavachin might affect the insulin sensitivity in vitro.

Bavachin ameliorates HFD-induced hepatic steatosis

We further explored the protective effect of bavachin on HFD-induced NAFLD. The mice were fed a HFD for 12 weeks and were subsequently maintained on the HFD and administered bavachin (30 mg/kg body weight every second day) intraperitoneally for 8 weeks (a total of 20 weeks on the HFD). Our results showed that bavachin treatment for 8 weeks significantly decreased the body weight of HFD-fed mice compared to that of control groups (Fig. 3a, b). Notably, bavachin caused a greater weight reduction

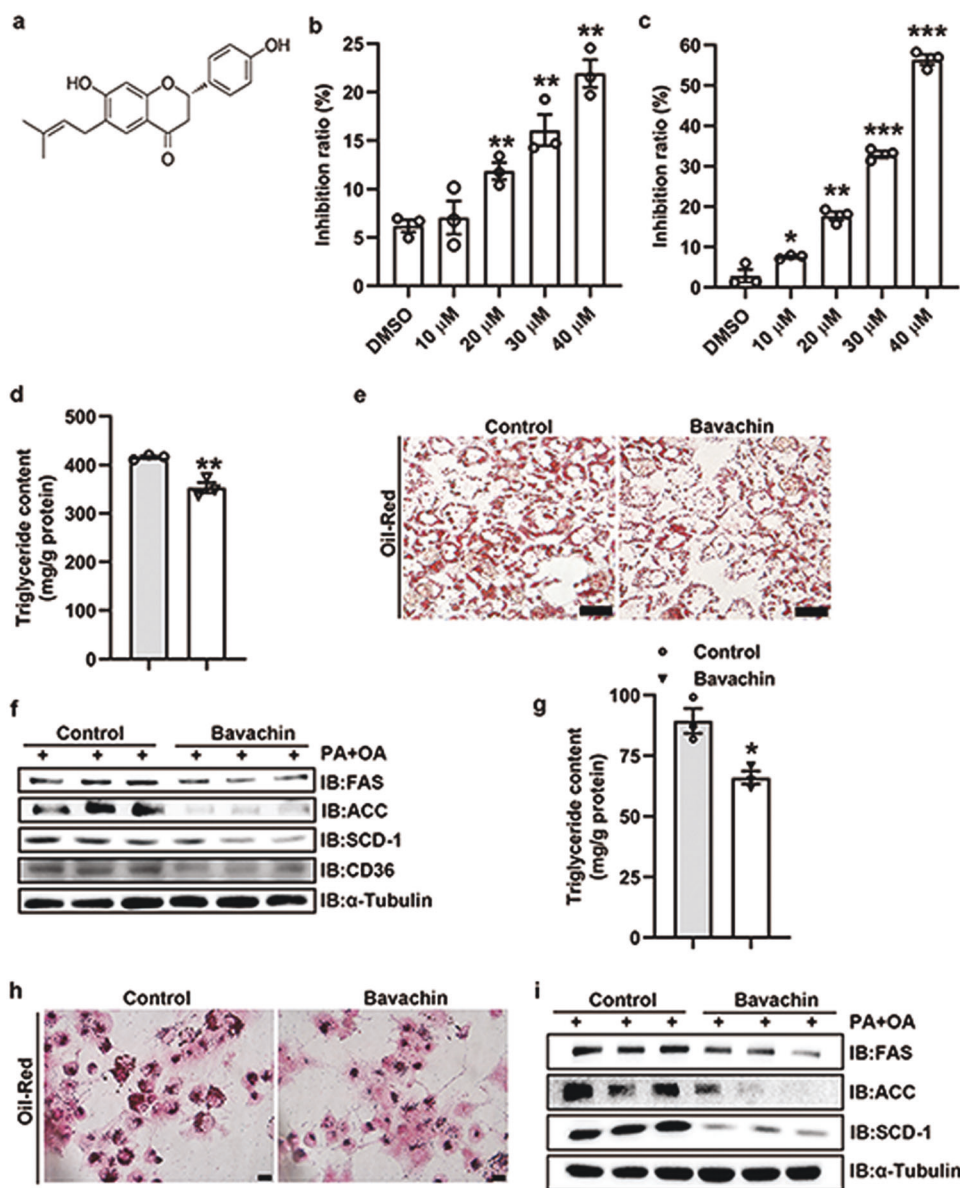


Fig. 1 Bavachin attenuates lipid accumulation in primary mouse hepatocytes and Huh7 cells. **a** Chemical structure of bavachin. MTT was used to detect the effect of different bavachin concentrations on the cytotoxicity of primary mouse hepatocytes **b** and Huh7 cells **c**. **d** TG content of primary mouse hepatocytes after PA/OA stimulation with or without bavachin treatment. **e** Oil Red O staining of primary mouse hepatocytes after PA/OA stimulation with or without bavachin treatment. **f** Western blot analysis of proteins involved in lipogenesis and fatty acid transport in primary mouse hepatocytes after PA/OA stimulation with or without bavachin treatment. **g** TG content of Huh7 cells after PA/OA stimulation with or without bavachin treatment. **h** Oil Red O staining of Huh7 cells after PA/OA stimulation with or without bavachin administration. **i** Western blot analysis of proteins involved in lipogenesis and fatty acid transport in Huh7 cells after PA/OA stimulation with or without bavachin administration. Data are presented as mean ± SEM; **P* < 0.05, ***P* < 0.01, ****P* < 0.001 by Student's *t*-test.

as compared to that caused by the HMG-CoA reductase inhibitor rosuvastatin calcium (Fig. 3b). Treatment with bavachin also effectively reduced the liver to body weight ratio (Fig. 3f); however, there was no difference in the daily food intake between the bavachin and control groups (Fig. 3e). Chronic HFD exposure induces hepatic steatosis, which involves the massive accumulation of large lipid droplets and ballooning degeneration of liver cells, which were alleviated by bavachin administration at 8 weeks. Hematoxylin and eosin (H&E) and Oil Red O staining revealed smaller lipid droplets and lesser degrees of ballooning degeneration in the hepatocytes of bavachin-treated mice compared with those of control groups (Fig. 3c, d). Biochemical analysis revealed that bavachin reduced the levels of serum TG, TC, and FFA compared to those in the control groups (Fig. 3g–i). However, after

bavachin treatment, only TG was significantly reduced in the liver, and although TC was decreased, the difference was not statistically significant (Fig. 3j, k). We further measured the hepatic VLDL secretion following tyloxapol injection, and observed that bavachin treatment in HFD-induced obesity reduced the liver lipoprotein production (Fig. 3l), which contributed to the increase in the serum TG content. These results indicate that bavachin can improve HFD-induced hepatic steatosis and reduce hepatic lipid accumulation.

The mechanism of action of bavachin in the regulation of liver lipid metabolism
To explore the potential mechanisms by which bavachin affects the lipid metabolism in mice, we performed RNA-seq experiments

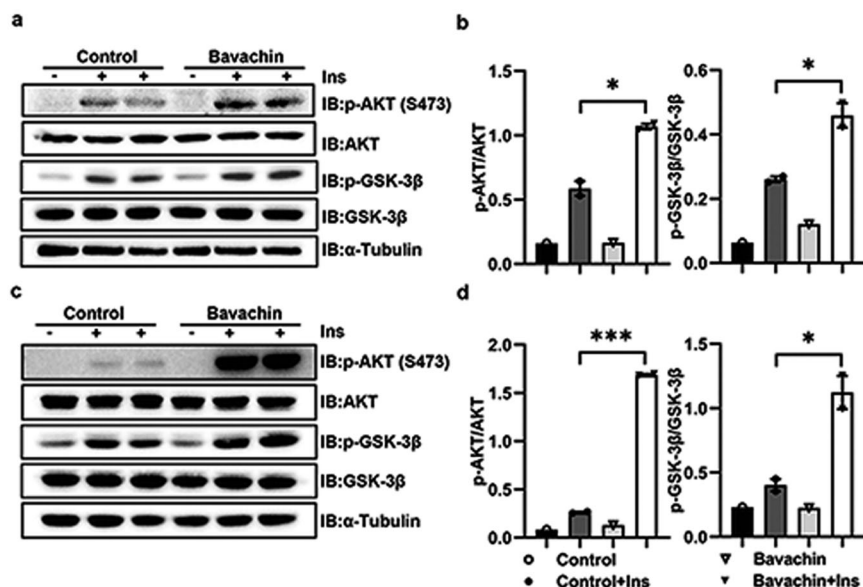


Fig. 2 Bavachin improves insulin sensitivity *in vitro*. **a** AKT and GSK-3 β phosphorylation were analysed by Western blot in primary mouse hepatocytes exposed to solvent or bavachin (20 μ M) for 24 h and subsequently treated with 100 nM Insulin (Ins) for 5 min. **b** AKT and GSK-3 β phosphorylation densitometry in **a**. **c** AKT and GSK-3 β phosphorylation were analysed by Western blot in Huh7 cells exposed to solvent or bavachin (20 μ M) for 24 h then treated with 100 nM Insulin (Ins) for 5 min. **d** AKT and GSK-3 β phosphorylation densitometry in **c**. Data are presented as mean \pm SEM; * P < 0.05, *** P < 0.001 by Student's *t*-test.

on liver tissue from mice in the bavachin and control groups. First, the volcano plot revealed that bavachin treatment resulted in a number of differentially expressed genes; 134 genes were downregulated, and 60 were upregulated after bavachin treatment (Fig. 4a). The Kyoto Encyclopedia of Genes and Genomes (KEGG) pathway analysis showed that bavachin could regulate liver lipid metabolism in HFD-induced obese mice (Fig. 4b). The heat map demonstrated the changes in genes were associated with lipid metabolism. The downregulated cluster was enriched for genes involved in lipid synthesis, accumulation, and transport (Fig. 4c). qPCR analysis indicated that the expression of lipogenic genes, such as sterol regulatory element-binding protein-1c (SREBP-1c), PPAR γ , SCD-1, and FAS, were significantly downregulated in the liver of HFD mice following bavachin treatment (Fig. 4d). We further observed that the expression of genes encoding CD36 and microsomal TG transfer protein (MTTP) were significantly reduced after bavachin treatment in the liver of HFD-induced obese mice compared with those in the control group (Fig. 4d). In contrast, bavachin increased the messenger ribonucleic acid (mRNA) levels of β -oxidation genes, including carnitine palmitoyl transferase I α (CPT-1 α), in the liver of HFD-induced obese mice (Fig. 4d). Immunoblot analysis further revealed that bavachin treatment resulted in lower protein levels of FAS, ACC, SCD-1, CD36, and MTTP but a higher CPT-1 α protein expression in the liver of HFD obese mice (Fig. 4e). Furthermore, we found that the mRNA and protein levels of perilipin2 (PLIN2) were markedly decreased in the bavachin groups compared to those in the control groups (Fig. 4d, e). PLIN2 expression strongly correlated with the steatosis severity. Additionally, transmission electron microscope (TEM) revealed an increase in the number of mitochondria and a more complete mitochondrial structure in the bavachin groups compared to untreated controls, while the structure of the hepatic endoplasmic reticulum was more intact and clear in the bavachin groups (Fig. 4f). Notably, we also observed that bavachin decreased the phosphorylation levels of inositol requiring 1 α (IRE-1 α) and eukaryotic initiation factor 2 α (eIF-2 α), as well as the protein expression of X-box binding protein 1 (XBP1) and C/EBP homologues protein (CHOP) compared to the control groups (Fig. 4g).

Autophagy is a major regulator of hepatic TG levels; to determine whether bavachin treatment affected autophagy activation in the liver, we assessed the expression of autophagy-related proteins in the livers of HFD-induced obese mice. The protein levels of p62 decreased significantly, and the light chain 3 (LC3) turnover increased in the bavachin group compared with those in the control groups (Fig. 4h). These data suggest that bavachin inhibits the expression of lipid synthesis genes in the liver of HFD-induced obese mice and confirmed that bavachin inhibited the expression of lipid synthesis genes in the livers of HFD-induced obese mice. Additionally, bavachin treatment increased the liver autophagy and improved the ER stress in obese mice.

Bavachin improves glucose homeostasis and insulin resistance in obesity induced by HFD

Bavachin treatment significantly decreased the blood glucose levels in HFD-induced obese mice (Fig. 5a). We subsequently performed GTT and ITT tests to investigate whether bavachin could improve the glucose homeostasis and insulin resistance in HFD-fed mice. Our results revealed that mice treated with bavachin displayed improved glucose homeostasis (Fig. 5b) and insulin sensitivity (Fig. 5c) relative to control mice. Moreover, the mice in the bavachin treatment group showed the same trend as that observed in the positive control group (Fig. 5b, c). The qPCR and Western blot results identified that the expression of G6Pase (glucose-6-phosphatase) was significantly reduced after bavachin treatment, while there was no significant change in PEPCK (phosphoenolpyruvate carboxykinase) (Fig. 5d, e). We further found that the phosphorylation of AKT on Ser473 was stronger in the liver (Fig. 5f, g), subcutaneous fat (Fig. 5h, i), and muscles (Fig. 5j, k) of HFD induced obese mice treated with bavachin compared to control mice. These findings suggest that bavachin treatment can ameliorate glucose homeostasis and insulin resistance in HFD-induced obese mice.

Bavachin treatment reduces hepatic inflammation induced by HFD

Hepatic inflammation plays a critical role in the progression of simple steatosis to NASH. Therefore, we explored the influence of

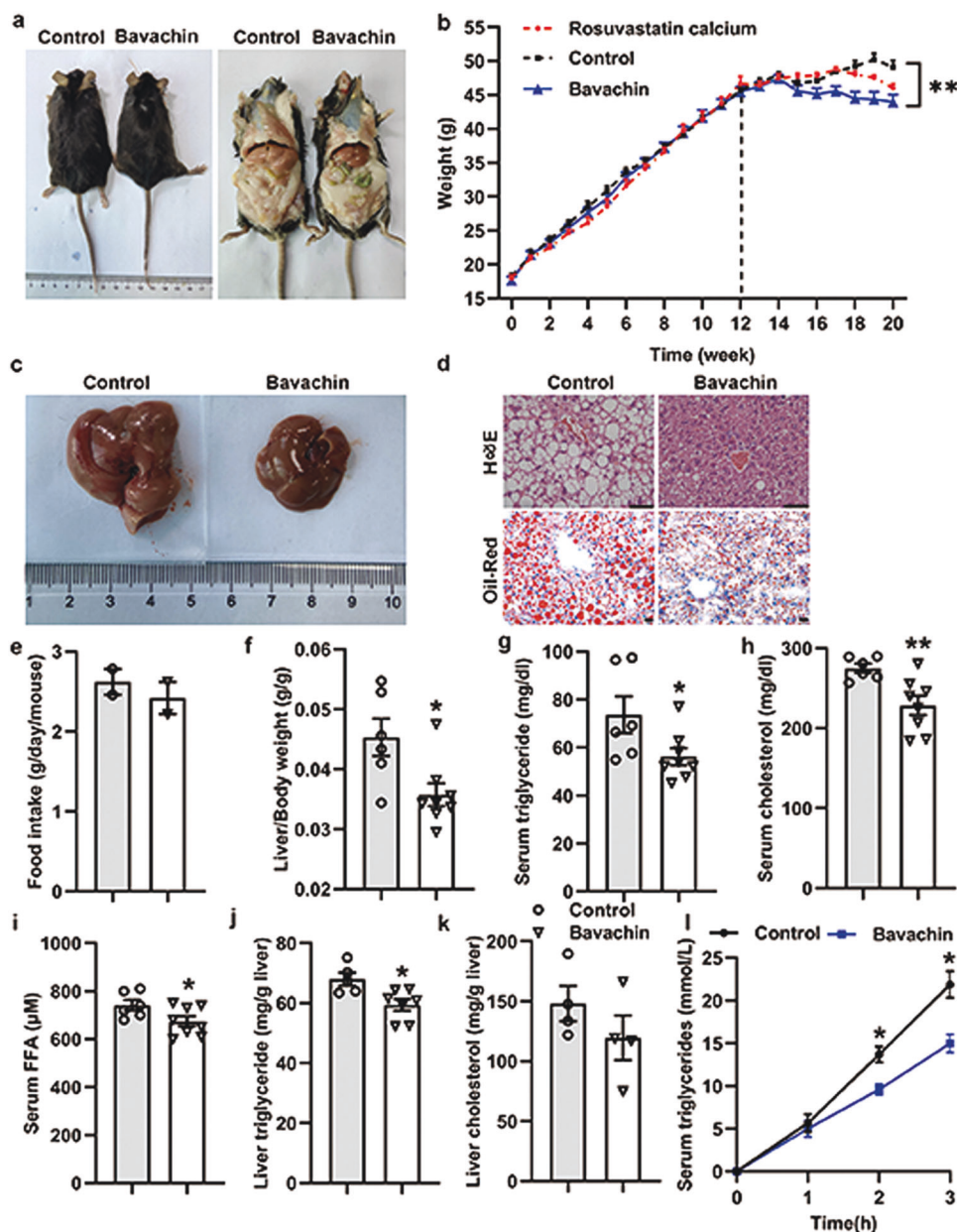


Fig. 3 Bavachin ameliorates hepatic steatosis caused by HFD feeding. **a** The representative gross morphology of mice fed a HFD at 0 for 20 weeks and treated with intraperitoneal bavachin at week 12 for 8 weeks. **b** The body weights of control and bavachin-treated mice were measured weekly from weeks 1–20. Representative results of **c** morphology, **d** H&E staining of sections (top panel), and Oil Red O staining (bottom panel) of livers from mice in the indicated groups; scale bars, 20 μ m. **e** Daily food intake of in the indicated mice. **f** The ratio of the liver weight to body weight in the indicated mice. **g–i** Changes in the fasting serum TG levels, TC levels and FFA levels in the indicated mice. **j, k** Changes in the fasting hepatic TG levels and TC levels in the indicated mice. **l** Hepatic VLDL-TG secretion in the indicated mice. Data are presented as mean \pm SEM; * P < 0.05, ** P < 0.01 by Student's *t*-test. One-way analysis of variance (ANOVA) was used to compare the three groups of data.

bavachin on hepatic inflammatory responses. Biochemical analysis confirmed that bavachin treatment significantly reduced the serum levels of ALT and AST in HFD-fed mice, while TNF α levels were significantly lower in the bavachin treatment group than in the non-treated group (Fig. 6a–c). We speculated that treatment with bavachin could ameliorate hepatic inflammation caused by the HFD. Meanwhile, qPCR revealed that the mRNA levels of proinflammatory factor genes, including TNF α , IL-6, and MCP1, were markedly reduced in the livers of HFD-induced obese mice after treatment with bavachin compared to those in the untreated groups (Fig. 6d). However, IL-1 β and NLRP3 had no significant

difference between the two groups (Fig. 6d). Moreover, immunohistochemical results revealed that the number of F4/80 positive cells was drastically reduced in the bavachin-treated liver compared to the vehicle controls, suggesting that bavachin results in less hepatic macrophage infiltration in HFD-induced obese mice (Fig. 6e). Additionally, Western blot analysis showed that the activation of c-Jun N-terminal kinase (JNK) and the phosphorylation levels of nuclear factor kappa B (NF- κ B) decreased after bavachin treatment (Fig. 6f). These results suggested that bavachin may exert a protective effect against HFD-induced hepatic inflammation.

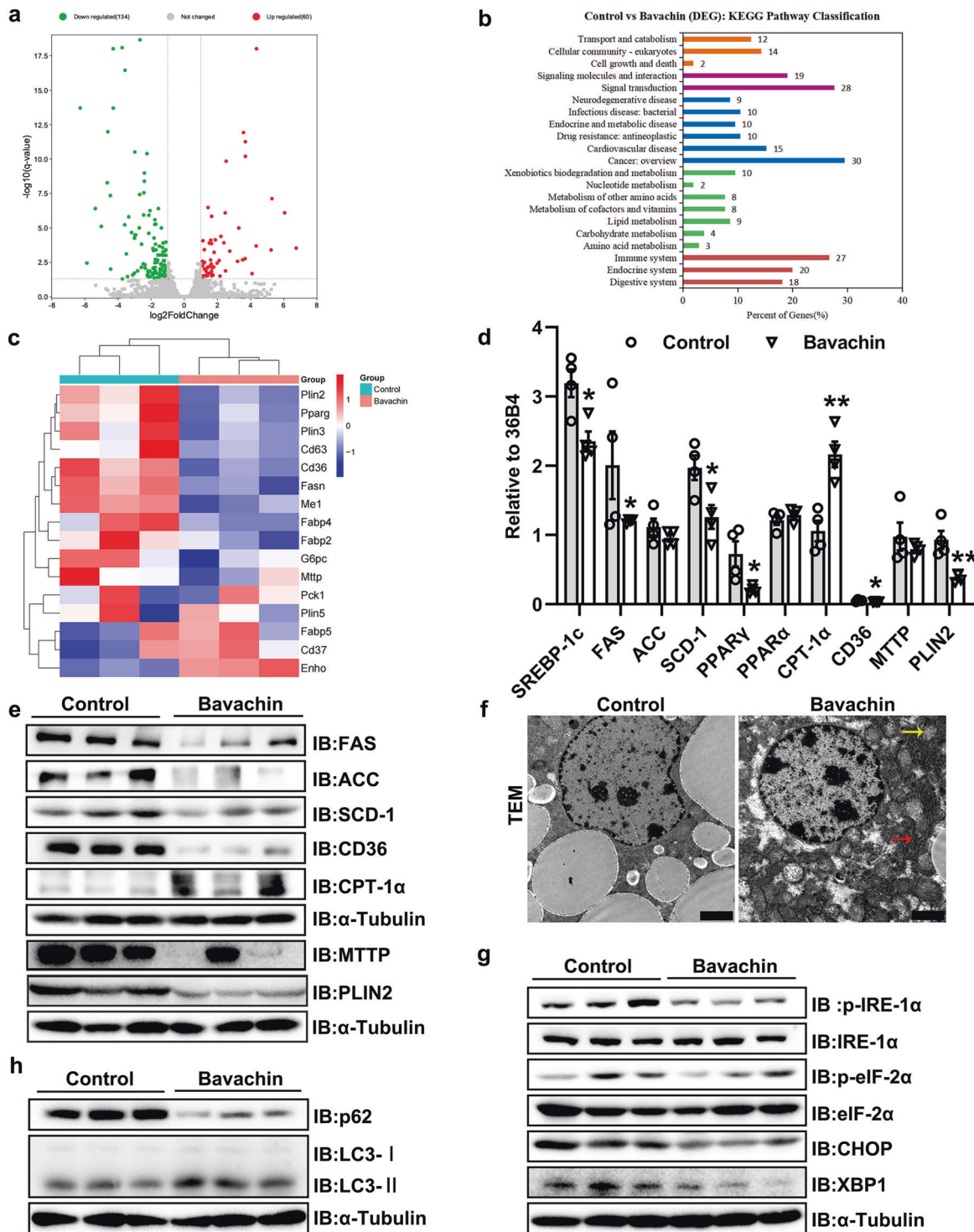


Fig. 4 Bavachin represses the hepatic lipogenesis in HFD-induced mice. **a** Scatterplot of differentially expressed genes identified by RNA-seq in the livers of 20 weeks HFD-fed mice with or without bavachin treatment. **b** KEGG pathway analysis showing the involved pathways of DEGs identified by RNA-seq. **c** Heatmap showing the expression of genes involved in hepatic lipid metabolism on RNA-seq. qPCR (**d**) and Western blot (**e**) analysis of genes involved in lipogenesis, fatty acid oxidation, and transport in the livers of control and bavachin-treated mice after 20 weeks of HFD. **f** Transmission EM observation of the hepatic microstructure, yellow arrows indicate the mitochondria, red arrows indicate the endoplasmic reticulum; scale bars, 2 μ m. **g** Western blot analysis of proteins involved in ER stress in the livers of control and bavachin-treated mice after 20 weeks of HFD. **h** Western blot analysis of proteins involved in autophagy in the livers of control and bavachin-treated mice after 20 weeks of HFD. Data are presented as the mean \pm SEM; * P < 0.05, ** P < 0.01, *** P < 0.001 by Student's *t*-test.

Bavachin protects against high-fat diet-induced obesity
Although bavachin-treated mice were resistant to HFD-induced obesity, with a body weight significantly lower than that in the non-

treatment group (Fig. 3b), we observed no difference in daily food intake between the two groups (Fig. 3e). Indeed, we measured and collected the corresponding adipose tissue. The results showed that

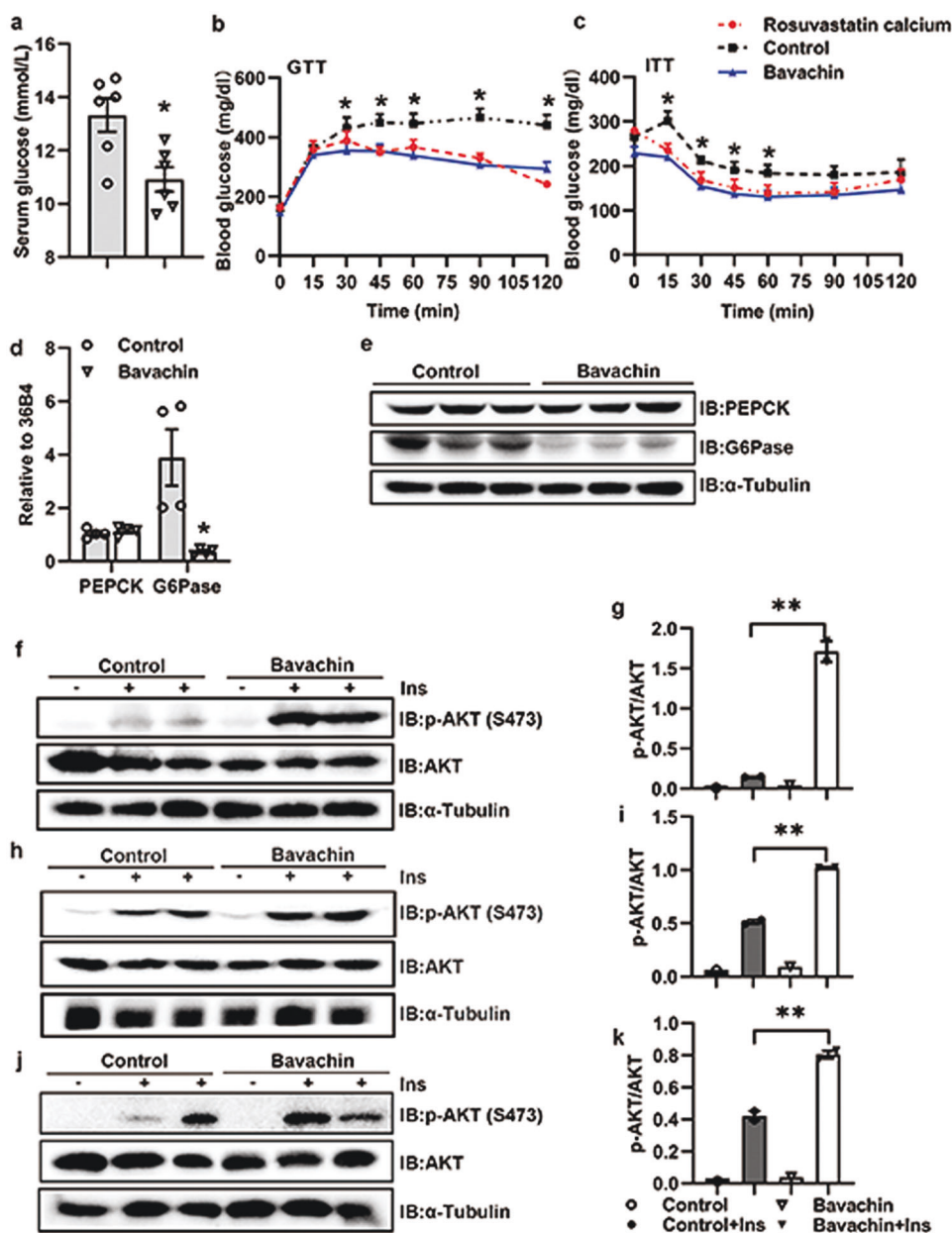


Fig. 5 Bavachin improves glucose homeostasis and insulin resistance in HFD-fed mice. **a** Blood glucose levels of control and bavachin-treated mice after 20 weeks of HFD followed by a 6 h fast. GTT analyses (**b**) and ITT analyses (**c**) were performed in control and bavachin-treated mice after 20 weeks of HFD. qPCR (**d**) and Western blot (**e**) were used to analyze the expression of gluconeogenic genes in the liver of control and bavachin-treated mice after 20 weeks of HFD. **f** Western blot analysis of insulin-stimulated AKT phosphorylation in the liver of control and bavachin-treated mice after 20 weeks of HFD. **g** Quantification of the Western blot data shown in **f**. **h** Western blot analysis of insulin-stimulated AKT phosphorylation in the subcutaneous fat tissue of control and bavachin-treated mice after 20 weeks of HFD. **i** Quantification of the Western blot data shown in **h**. **j** Western blot analysis of insulin-stimulated AKT phosphorylation in the muscle of control and bavachin-treated mice after 20 weeks of HFD. **k** Quantification of the Western blot data shown in **j**. Data are presented as mean \pm SEM; * $P < 0.05$, ** $P < 0.01$ by Student's *t*-test. One-way analysis of variance (ANOVA) was used to compare the three groups of data.

the subWAT mass and visceral adipose tissue (VAT) mass were markedly reduced in obese mice treated with bavachin compared to control mice, whereas the epididymal white adipose tissue (epiWAT) mass did not differ between the two groups (Fig. 7a). Histological analysis revealed that the size of adipocytes in the subWAT, VAT, and BAT of mice fed an HFD treated with bavachin was reduced compared with the control mice (Fig. 7b, f and Supplementary Fig. S4a, c). Interestingly, we observed an increase in the rectal body temperature in bavachin-treated mice compared to the control group (Fig. 7c). Thus, we speculated that bavachin might either promote the browning/beiging of subWAT or increase BAT activity.

Furthermore, we detected the expression profiles of genes linked to thermogenesis, beiging, and mitochondrial respiration in the subWAT and BAT. qPCR analysis showed that the induction of thermogenesis, beiging, and mitochondrial respiration marker genes such as uncoupling protein 1 (UCP1), PR domain-containing 16 (Prdm16), Cidea, and peroxisome proliferator-activated receptor γ coactivator 1 α (PGC-1 α) were significantly upregulated in the subWAT and BAT of mice that were fed an HFD and treated with bavachin compared with the untreated mice (Fig. 7d–g). Moreover, Western blotting also verified that the protein levels of UCP1 and PGC-1 α were significantly increased in both the subWAT and BAT of

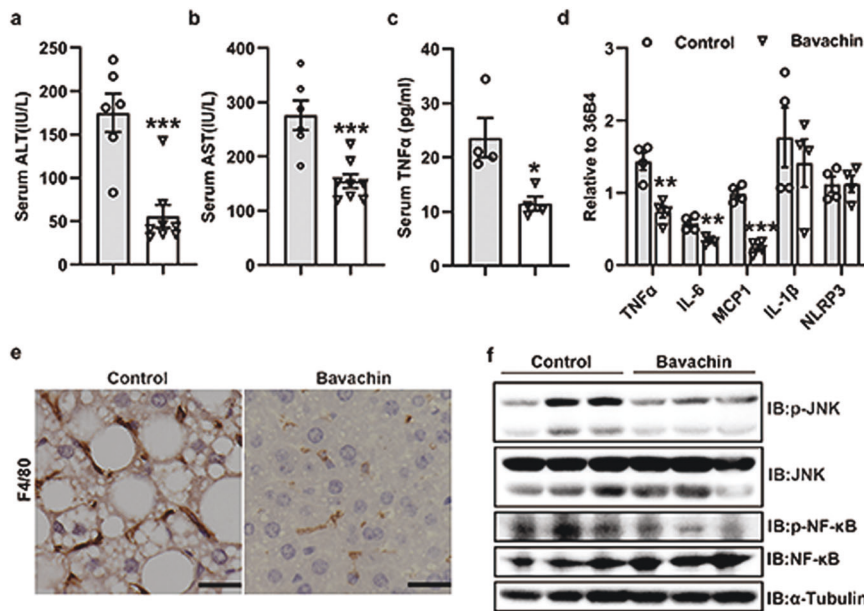


Fig. 6 Bavachin alleviates HFD-induced hepatic inflammation. Serum ALT (a), AST (b) and TNF α (c) levels of control and bavachin-treated mice after 20 weeks of HFD followed by a 6 h fast. **d** mRNA expression of pro-inflammatory cytokines in the liver of control and bavachin-treated mice after 20 weeks of the HFD. **e** Histological F4/80 staining in liver sections of control and bavachin-treated mice fed a HFD for 20 weeks; scale bars, 25 μ m. **f** Western blot analysis of JNK and NF- κ B protein and phosphorylation levels in the liver of control and bavachin-treated mice after 20 weeks of the HFD. Data are presented as mean \pm SEM; * P < 0.05, ** P < 0.01, *** P < 0.001 by Student's *t*-test.

HFD-fed mice after treatment with bavachin compared with the control mice (Fig. 7e–h). In addition, we also found that bavachin was involved in the regulation of lipid synthesis and fatty acid oxidation genes in the subWAT of HFD-fed mice, showing an inhibition of FAS expression and promotion of peroxisome proliferator-activated receptor α (PPAR α) and CPT-1 α expressions (Supplementary Fig. S4d). These findings suggest that bavachin may protect against HFD-induced obesity by inducing fat thermogenesis and beige subWAT.

DISCUSSION

Although significant progress has been made in clarifying the pathogenesis of NAFLD, identifying therapeutic targets, and advancing treatment strategies, several aspect challenges are still unclear. Most notably, there are currently no drugs approved to treat this condition. However, the beneficial effects of traditional Chinese medicine on metabolic diseases continue to be demonstrated, prompting researchers to seek potentially effective and safe treatments using traditional Chinese medicine.

Psoralea corylifolia L. (Fabaceae) (PC) is a widely used pleiotropic medicinal herb [17] with its major constituents being bakuchiol, psoralen, bavachin, corylifolin, coumarins, daidzin, and corylin. PC causes several pharmacological effects, including anti-oxidant, anti-tumor, anti-bacterial, and protective effects on cutaneous conditions, impotence, and hepatic injury [18]. In addition, PC extract has been shown to exert anti-hyperglycemic effects in rats by increasing their serum insulin levels and decreasing their blood glucose levels [17]. Bavachin has also been reported to exhibit multiple pharmacological actions, including anti-bacterial [19], osteoblastic activity [20] and anti-tumor effects [21]. However, the effects of bavachin on NAFLD remain unclear.

In this study, our data verified that bavachin treatment significantly reduced the body weight of HFD-fed mice compared to that of untreated controls. Moreover, we found that bavachin treatment not only reduced the liver TG content induced by an HFD, but also reduced the serum TG content, as well as the hepatic VLDL secretion. De novo lipogenesis (DNL) plays an

important role in the development of hepatic steatosis. Increased DNL stimulates the expression of the transcription factor SREBP-1c and carbohydrate-responsive element-binding protein (ChREBP), which in turn increases the expression of certain genes in the FA biosynthetic pathway, including FAS, ACC, and SCD-1 [13, 22]. In addition, the DNL pathway increases lipid synthesis, fatty acid oxidation, and lipid secretion, and its modulation also plays an important role in hepatic lipid accumulation. Our study demonstrated that bavachin treatment in HFD mice resulted in a decrease in the expression of genes related to DNL and lipid translocation, as well as an increase in CPT-1 α , which is closely linked to fatty acid oxidation. Thus, the combined effect of increased fatty acid oxidation and decreased lipid synthesis in the liver of bavachin-treated mice may be partly responsible for alleviating fatty liver in mice. Although our results confirmed that bavachin treatment could inhibit the secretion of VLDL in liver, the TG content in liver of mice after bavachin treatment was still decreased compared with that of the control group due to the reduced total TG synthesis in the liver. Primary hepatocytes of mice and Huh7 cells were similarly exposed to PA/OA in vitro, and after bavachin treatment, lipid droplets were reduced and TG content was decreased.

Previous studies have indicated that PLIN2 is the most abundant member of the perilipin protein family, which is involved in the steatotic livers of mice and humans and its expression is strongly associated with the severity of steatosis [23, 24]. Previous studies have demonstrated that deletion of PLIN2 is associated with a lower hepatic TG, enhanced insulin sensitivity, and improved glucose homeostasis [25, 26], whereas hepatic overexpression of PLIN2 increases the cellular TG and lipid droplet size, with a reduction in lipolysis [27]. Growing evidence has shown that hepatic steatosis is determined by de novo lipogenesis, lipid uptake, fatty acid β -oxidation, and VLDL secretion [28]. Our study confirmed that bavachin can indeed reduce the PLIN2 protein levels in the liver of HFD-induced mice. In addition, deletion of PLIN2 can increase liver autophagy in obese mice, thus reducing the hepatic TG content [29]. Hepatic lipid accumulation is linked to insulin resistance, mitochondrial

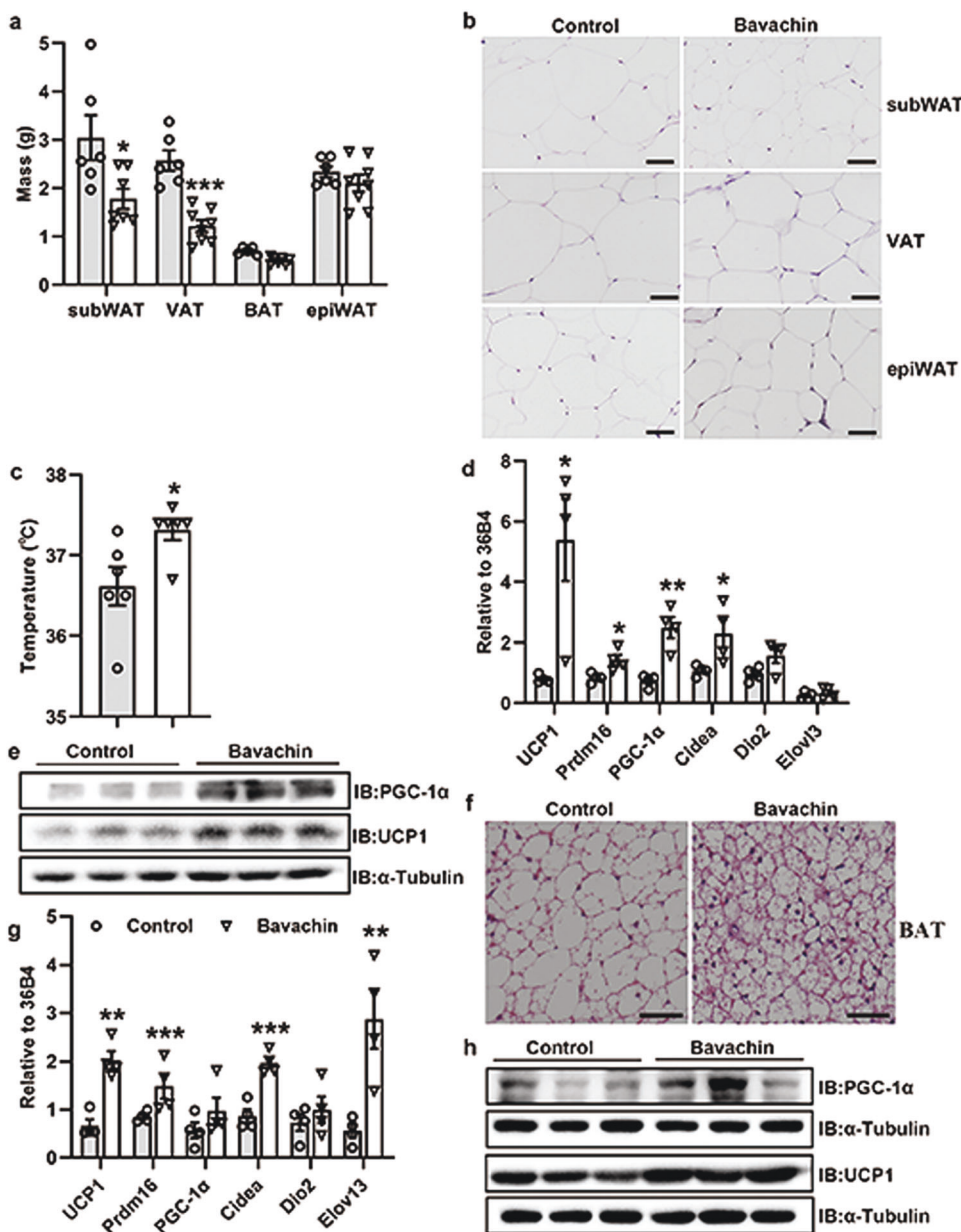


Fig. 7 Bavachin increases thermogenesis and browning of the white adipose tissue in mice fed HFD. **a** The weight of different fat pads in control and bavachin-treated mice fed a HFD for 20 weeks. **b** H&E staining of subWAT, VAT, and epiWAT of control and bavachin-treated mice; scale bars, 50 μ m. **c** Rectal body temperature in control and bavachin-treated mice. **d** qPCR analysis of genes involved in thermogenesis, beiging, and mitochondrial respiration in the subWAT of control and bavachin-treated mice after 20 weeks of HFD. **e** Western blot analysis of UCP1 and PGC-1 α protein levels in the subWAT of control and bavachin-treated mice after 20 weeks of HFD. **f** H&E staining of the BAT of control and bavachin-treated mice; scale bars, 50 μ m. **g** qPCR analysis of genes involved in thermogenesis, beiging, and mitochondrial respiration in the BAT of control and bavachin-treated mice after 20 weeks of HFD. **h** Western blot analysis of UCP1 and PGC-1 α protein levels in the BAT of control and bavachin-treated mice after 20 weeks of HFD. Data are presented as mean \pm SEM; * P < 0.05, ** P < 0.01, *** P < 0.001 by Student's t -test.

stress, impaired autophagy, and ER stress, eventually triggering NAFLD [30]. Previous reports have indicated a link between chronic ER stress and obesity, as established by the presence of ER stress markers in steatotic livers of HFD-fed mice [31]. Excessive accumulation of TG in hepatocytes degrades the intracellular lipid droplets through lipid specific autophagy, termed lipophagy [32]. Our results confirmed that bavachin treatment ameliorated the hepatic ER stress induced by an HFD and increased hepatic autophagy. However, a previous study reported that bavachin induces apoptosis through the upregulation of ER stress in HepG2 cells [21]. This contrasting result may

be due to the difference in cellular environments and physiological states.

Bavachin has been reported to inhibit cell proliferation and induce apoptosis by inducing cytotoxicity in HepG2 cells [21]. However, our study demonstrated that low concentrations of bavachin were less toxic to primary mouse hepatocytes. Few studies have claimed that bavachin can enhance the activation of inflammatory vesicles to increase hepatotoxicity, while others have indicated that bavachin attenuates lipopolysaccharide lipopolysaccharide-induced inflammatory response and inhibits the activation of the NOD-, LRR- and pyrin domain-containing 3

(NLRP3) inflammasome in macrophages [33, 34]. Liver inflammation is a determinant of the NAFLD to NASH progression. Compared to control groups, the serum levels of ALT and AST in the HFD-bavachin groups were significantly decreased, while the serum levels of TNF α in bavachin-treated mice were significantly reduced. These changes were accompanied by a decrease in F4/80 macrophages in the livers of HFD-induced obese mice after treatment with bavachin compared to the control group. The regulatory effects of HFD on the expression of inflammatory genes such as TNF α , IL-6 and MCP1, were abolished on treatment with bavachin. Moreover, our results indicated that the JNK and NF- κ B pathways were significantly suppressed by bavachin administration in the liver of HFD-induced obese mice. These data indicated that bavachin prevents liver injury by alleviating hepatic inflammation. However, the inhibitory effects of bavachin on NASH progression require further investigation.

Several drugs have been shown to improve the hepatic insulin resistance and NAFLD by modulating the cellular energy balance [35]. This modulation is a key feature of these drugs, and has been reported to reduce liver fat and/or improve liver insulin sensitivity [36, 37]. Herein, we demonstrated that bavachin ameliorated HFD-induced insulin resistance in the liver and adipose tissue. Moreover, bavachin treatment improved the glucose homeostasis in HFD-fed obese mice and decreased their blood glucose levels, which is also reported in previous studies [38].

No difference in the daily food intake between the two groups was reported; however, the body weight of the mice in the bavachin group was significantly lower than that of the control group. Notably, BAT is the primary site for uncoupled respiration-mediated thermogenesis [39], and activated BAT ameliorates NAFLD and enhances the beneficial effects of calorie restriction in improving steatohepatitis in mice [40, 41]. Furthermore, browning of WAT has beneficial effects against obesity and related disorders, similar to those observed following BAT activation [42, 43]. Obese mice treated with bavachin had lower subcutaneous and visceral fat than the control group. The body temperatures of HFD-fed mice treated with bavachin was slightly higher than that of control group, suggesting that protection from obesity in bavachin-treated mice is most likely related to increased energy expenditure. Our study also demonstrated that the expression levels of the thermogenic markers UCP1, Prdm16, PGC-1 α , and Cidea were markedly upregulated in BAT and subWAT of bavachin-treated HFD-fed mice compared to controls, suggesting that bavachin enhanced the activation of the thermogenic program. Future studies to identify the precise mechanisms underlying this effect will be of interest.

Overall, our study showed that bavachin could ameliorate NAFLD caused by HFD by reducing DNL. Meanwhile, bavachin promotes energy metabolism, such as beige adipocyte formation and browning of the subWAT. The present study provides evidence of the beneficial effects of bavachin in the treatment of obesity-related NAFLD.

ACKNOWLEDGEMENTS

This work was supported by collective grants from the National Natural Science Foundation of China (No. 81870402 and 81670517), Anhui Science Fund for Distinguished Young Scholars (No. 2208085J45), Key Research and Development Program of Anhui Province (No. 2022i01020023), Research Fund of Anhui Institute of translational medicine (No. 2022zhyx-C12) and the Project Funded by Scientific Research Platform and Base Upgrading Plan of Anhui Medical University (No. 2021xkjT048).

AUTHOR CONTRIBUTIONS

HBZ and MZ designed the research and revised the paper. XW, LL, QQY, XYW, QZ, XMZ, KCT, MYG, TYD, WH, DKH and YLQ performed experiments. XW and HBZ analysed the data. XW wrote the paper. HBZ and MZ reviewed the paper.

ADDITIONAL INFORMATION

Supplementary information The online version contains supplementary material available at <https://doi.org/10.1038/s41401-023-01056-z>.

Competing interests: The authors declare no competing interests.

REFERENCES

1. Cotter TG, Rinella M. Nonalcoholic fatty liver disease 2020: the state of the disease. *Gastroenterology*. 2020;158:1851–64.
2. Overi D, Carpino G, Franchitto A, Onori P, Gaudio E. Hepatocyte injury and hepatic stem cell niche in the progression of non-alcoholic steatohepatitis. *Cells*. 2020;9:590.
3. Younossi ZM, Koenig AB, Abdelatif D, Fazel Y, Henry L, Wymer M. Global epidemiology of nonalcoholic fatty liver disease—Meta-analytic assessment of prevalence, incidence, and outcomes. *Hepatology*. 2016;64:73–84.
4. Friedman SL, Neuschwander-Tetri BA, Rinella M, Sanyal AJ. Mechanisms of NAFLD development and therapeutic strategies. *Nat Med*. 2018;24:908–22.
5. Liu ZL, Xie LZ, Zhu J, Li GQ, Grant SJ, Liu JP. Herbal medicines for fatty liver diseases. *Cochrane Database Syst Rev*. 2013;8:D9059.
6. Zhou H, Ma C, Wang C, Gong L, Zhang Y, Li Y. Research progress in use of traditional Chinese medicine monomer for treatment of non-alcoholic fatty liver disease. *Eur J Pharmacol*. 2021;898:173976.
7. Hosseini H, Teimouri M, Shabani M, Koushki M, Babaei KR, Namvarjah F, et al. Resveratrol alleviates non-alcoholic fatty liver disease through epigenetic modification of the Nrf2 signaling pathway. *Int J Biochem Cell Biol*. 2020;119:105667.
8. Yan C, Zhang Y, Zhang X, Aa J, Wang G, Xie Y. Curcumin regulates endogenous and exogenous metabolism via Nrf2-FXR-LXR pathway in NAFLD mice. *Biomed Pharmacother*. 2018;105:274–81.
9. Li Y, Qiao J, Wang B, Bai M, Shen J, Cheng Y. Paeoniflorin ameliorates fructose-induced insulin resistance and hepatic steatosis by activating LKB1/AMPK and AKT pathways. *Nutrients*. 2018;10:1024.
10. Liu J, Yuan Y, Gong X, Zhang L, Zhou Q, Wu S, et al. Baicalin and its nanoliposomes ameliorates nonalcoholic fatty liver disease via suppression of TLR4 signaling cascade in mice. *Int Immunopharmacol*. 2020;80:106208.
11. Wang S, Yang FJ, Shang LC, Zhang YH, Zhou Y, Shi XL. Puerarin protects against high-fat high-sucrose diet-induced non-alcoholic fatty liver disease by modulating PARP-1/PI3K/AKT signaling pathway and facilitating mitochondrial homeostasis. *Phytother Res*. 2019;33:2347–59.
12. Lu Z, He B, Chen Z, Yan M, Wu L. Anti-inflammatory activity of berberine in non-alcoholic fatty liver disease via the Angptl2 pathway. *BMC Immunol*. 2020;21:28.
13. Zhu X, Bian H, Wang L, Sun X, Xu X, Yan H, et al. Berberine attenuates non-alcoholic hepatic steatosis through the AMPK-SREBP-1c-SCD1 pathway. *Free Radic Biol Med*. 2019;141:192–204.
14. Wan J, Zhang Y, Yang D, Liang Y, Yang L, Hu S, et al. Gastrodin improves non-alcoholic fatty liver disease through activation of the adenosine monophosphate-activated protein kinase signaling pathway. *Hepatology*. 2021;74:3074–90.
15. Hu M, Zhang D, Xu H, Zhang Y, Shi H, Huang X, et al. Salidroside activates the AMP-activated protein kinase pathway to suppress nonalcoholic steatohepatitis in mice. *Hepatology*. 2021;74:3056–73.
16. Chopra B, Dhingra AK, Dhar KL. *Psoralea corylifolia* L. (Buguchi) - folklore to modern evidence: review. *Fitoterapia*. 2013;90:44–56.
17. Lee H, Li H, Noh M, Ryu J. Bavachin from *Psoralea corylifolia* improves insulin-dependent glucose uptake through insulin signaling and AMPK activation in 3T3-L1 adipocytes. *Int J Mol Sci*. 2016;17:527.
18. Khushboo PS, Jadhav VM, Kadam VJ, Sathe NS. *Psoralea corylifolia* Linn.—“Kush-tanashini”. *Pharmacogn Rev*. 2010;4:69.
19. Ávila HP, Smânia EDFA, Monache FD, Smânia A. Structure-activity relationship of antibacterial chalcones. *Bioorg Med Chem*. 2008;16:9790–94.
20. Weng Z, Gao Q, Wang F, Zhao G, Yin F, Cai B, et al. Positive skeletal effect of two ingredients of *Psoralea corylifolia* L. on estrogen deficiency-induced osteoporosis and the possible mechanisms of action. *Mol Cell Endocrinol*. 2015;417:103–13.
21. Yang Y, Tang X, Hao F, Ma Z, Wang Y, Wang L, et al. Bavachin induces apoptosis through mitochondrial regulated ER stress pathway in HepG2 cells. *Biol Pharm Bull*. 2018;41:198–207.
22. Ameer F, Scanduzzi L, Hasnain S, Kalbacher H, Zaidi N. De novo lipogenesis in health and disease. *Metabolism*. 2014;63:895–902.
23. McManaman JL, Bales ES, Orlicky DJ, Jackman M, MacLean PS, Cain S, et al. Perilipin-2-null mice are protected against diet-induced obesity, adipose inflammation, and fatty liver disease. *J Lipid Res*. 2013;54:1346–59.
24. Straub BK, Stoeffel P, Heid H, Zimbelmann R, Schirmacher P. Differential pattern of lipid droplet-associated proteins and de novo perilipin expression in hepatocyte steatogenesis. *Hepatology*. 2008;47:1936–46.
25. Chang BH, Li L, Saha P, Chan L. Absence of adipose differentiation related protein upregulates hepatic VLDL secretion, relieves hepatosteatosis, and improves

- whole body insulin resistance in leptin-deficient mice. *J Lipid Res.* 2010;51:2132–42.
26. Chang BH, Li L, Paul A, Taniguchi S, Nannegari V, Heird WC, et al. Protection against fatty liver but normal adipogenesis in mice lacking adipose differentiation-related protein. *Mol Cell Biol.* 2006;26:1063–76.
 27. Imamura M, Inoguchi T, Ikuyama S, Taniguchi S, Kobayashi K, Nakashima N, et al. ADRP stimulates lipid accumulation and lipid droplet formation in murine fibroblasts. *Am J Physiol Endocrinol Metab.* 2002;283:E775–83.
 28. Liu Y, Jiang L, Sun C, Ireland N, Shah YM, Liu Y, et al. Insulin/Snail1 axis ameliorates fatty liver disease by epigenetically suppressing lipogenesis. *Nat Commun.* 2018;9:2751.
 29. Tsai T, Chen E, Li L, Saha P, Lee H, Huang L, et al. The constitutive lipid droplet protein PLIN2 regulates autophagy in liver. *Autophagy.* 2017;13:1130–44.
 30. Lebeaupin C, Vallée D, Hazari Y, Hetz C, Chevet E, Bailly-Maitre B. Endoplasmic reticulum stress signalling and the pathogenesis of non-alcoholic fatty liver disease. *J Hepatol.* 2018;69:927–47.
 31. Gregor MF, Yang L, Fabbrini E, Mohammed BS, Eagon JC, Hotamisligil GS, et al. Endoplasmic reticulum stress is reduced in tissues of obese subjects after weight loss. *Diabetes.* 2009;58:693–700.
 32. Schulze RJ, Sathyanarayan A, Mashek DG. Breaking fat: The regulation and mechanisms of lipophagy. *Biochim Biophys Acta Mol Cell Biol Lipids.* 2017;1862:1178–87.
 33. Qin N, Xu G, Wang Y, Zhan X, Gao Y, Wang Z, et al. Bavachin enhances NLRP3 inflammasome activation induced by ATP or nigericin and causes idiosyncratic hepatotoxicity. *Front Med.* 2021;15:594–607.
 34. Hung Y, Wang S, Suzuki K, Fang S, Chen C, Cheng W, et al. Bavachin attenuates LPS-induced inflammatory response and inhibits the activation of NLRP3 inflammasome in macrophages. *Phytomedicine.* 2019;59:152785.
 35. Samuel VT, Shulman GI. Nonalcoholic fatty liver disease as a nexus of metabolic and hepatic diseases. *Cell Metab.* 2018;27:22–41.
 36. Smith BK, Ford RJ, Desjardins EM, Green AE, Hughes MC, Houde VP, et al. Salsalate (Salicylate) uncouples mitochondria, improves glucose homeostasis, and reduces liver lipids independent of AMPK-beta1. *Diabetes.* 2016;65:3352–61.
 37. Lindquist C, Bjørndal B, Rossmann CR, Tusubira D, Svardal A, Røslund GV, et al. Increased hepatic mitochondrial FA oxidation reduces plasma and liver TG levels and is associated with regulation of UCPs and APOC-III in rats. *J Lipid Res.* 2017;58:1362–73.
 38. Krenisky JM, Luo J, Reed MJ, Carney JR. Isolation and antihyperglycemic activity of bakuchiol from *Otholobium pubescens* (Fabaceae), a Peruvian medicinal plant used for the treatment of diabetes. *Biol Pharm Bull.* 1999;22:1137–40.
 39. Tseng YH, Cypess AM, Kahn CR. Cellular bioenergetics as a target for obesity therapy. *Nat Rev Drug Discov.* 2010;9:465–82.
 40. Giles DA, Moreno-Fernandez ME, Stankiewicz TE, Graspeuntner S, Cappelletti M, Wu D, et al. Thermoneutral housing exacerbates nonalcoholic fatty liver disease in mice and allows for sex-independent disease modeling. *Nat Med.* 2017;23:829–38.
 41. Poekes L, Gillard J, Farrell GC, Horsmans Y, Leclercq IA. Activation of brown adipose tissue enhances the efficacy of caloric restriction for treatment of non-alcoholic steatohepatitis. *Lab Invest.* 2019;99:4–16.
 42. Cohen P, Levy JD, Zhang Y, Frontini A, Kolodin DP, Svensson KJ, et al. Ablation of PRDM16 and beige adipose causes metabolic dysfunction and a subcutaneous to visceral fat switch. *Cell.* 2014;156:304–16.
 43. Zhang X, Luo Y, Wang C, Ding X, Yang X, Wu D, et al. Adipose mTORC1 suppresses prostaglandin signaling and beige adipogenesis via the CRTC2-COX-2 pathway. *Cell Rep.* 2018;24:3180–93.

Springer Nature or its licensor (e.g. a society or other partner) holds exclusive rights to this article under a publishing agreement with the author(s) or other rightsholder(s); author self-archiving of the accepted manuscript version of this article is solely governed by the terms of such publishing agreement and applicable law.